Pre-melt-season sediment plume variability at Jokulsarlon, Iceland: a preliminary evaluation using in-situ spectroradiometry and satellite imagery

---

Pre-melt-season sediment plume variability at Jökulsárlón, Iceland, a preliminary evaluation using in-situ spectroradiometry and satellite imagery

Richard Hodgkins, Robert Bryant, Eleanor Darlington and Mark Brandon

Annals of Glaciology / *FirstView* Article / May 2016, pp 1 - 8
DOI: 10.1017/aog.2016.20, Published online: 12 May 2016

Annals of Glaciology (2016), Page 1 of 8 doi: 10.1017/aog.2016.20

Pre-melt-season sediment plume variability at Jökulsárlón, Iceland, a preliminary evaluation using in-situ spectroradiometry and satellite imagery

Richard HODGKINS,[1] Robert BRYANT,[2] Eleanor DARLINGTON,[1] Mark BRANDON[3]

[1]*Department of Geography, Loughborough University, Leicestershire LE11 3TU, UK*
E-mail: r.hodgkins@lboro.ac.uk
[2]*Department of Geography, University of Sheffield, Sheffield S10 2TN, UK*
[3]*Department of Environment, Earth & Ecosystems, Open University, Walton Hall, Milton Keynes MK7 6AA, UK*

ABSTRACT. High-latitude atmospheric warming is impacting freshwater cycling, requiring techniques for monitoring the hydrology of sparsely-gauged regions. The submarine runoff of tidewater glaciers presents a particular challenge. We evaluate the utility of Moderate Resolution Imaging Spectroradiometer (MODIS) imagery for monitoring turbid meltwater plume variability in the glacier lagoon Jökulsárlón, Iceland, for a short interval before the onset of the main melt season. Total Suspended Solids concentrations (*TSS*) of surface waters are related to remotely-sensed reflectance via empirical calibration between in-situ-sampled *TSS* and reflectance in a MODIS band 1-equivalent wavelength window. This study differs from previous ones in its application to an overturning tidewater glacier plume, rather than one derived from river runoff. The linear calibration improves on previous studies by facilitating a wider range of plume metrics than areal extent, notably pixel-by-pixel *TSS* values. Increasing values of minimum plume *TSS* over the study interval credibly represent rising overall turbidity in the lagoon as melting accumulates. Plume extent responds principally to consistently-strong offshore winds. Further work is required to determine the temporal persistence of the calibration, but remote plume observation holds promise for monitoring hydrological outputs from ungauged or ungaugeable systems.

KEYWORDS: atmosphere/ice/ocean interactions, fluvial transport, glacier hydrology, ice/ocean interactions, tidewater

INTRODUCTION

One of the most important ways in which Arctic hydrology is responding to rapid atmospheric warming is by changing the timing and magnitude of freshwater runoff to the marine environment, with potentially profound implications for coastal circulation, fluxes of sediment and nutrients to nearshore ecosystems and zooplankton productivity (Statham and others, 2008; Arendt and others, 2011). Within the high-latitude hydrologic cycle, glaciers play an important role in modulating river flow and in the delivery of sediments and solutes to lowlands and coasts. Atmospheric warming is driving increased runoff through enhanced rates of melting and through the lengthening of melt seasons, which is reflected in both widespread glacier retreat and augmented river flows. Globally, the stability of glaciers and ice sheets with marine margins is expected to be one of the most important factors contributing to 21st-century sea-level rise (Church and others, 2013). However, understanding of the hydrology of marine-terminating or tidewater glaciers lags behind that of their terrestrial counterparts (Joughin and others, 2012).

An abiding, fundamental problem is that runoff from tidewater glaciers emerges in an inaccessible, submarine location and therefore cannot be measured or monitored directly (Straneo and others, 2013). Yet this runoff is fresh, buoyant and often turbid; hence, it frequently forms observable, overturning plumes (Chu, 2013). These plumes are typically much wider than many river channels, and so more amenable to observation with remotely-sensed imagery. Their characteristics can therefore be measured and their variations tracked, which is of benefit for the study of both the large-scale hydrology of remote, ungauged (and ungaugeable) regions, and the stability and dynamics of large glaciers draining ice sheets.

Remote estuarine and coastal plume monitoring is already well established for non-glacial environments (e.g. Curran and Novo, 1988; Doxaran and others, 2002; Hu and others, 2004; Miller and McKee, 2004) but has only of late been applied to glacial ones (e.g. Chu and others, 2009, 2012; McGrath and others, 2010; Tedstone and Arnold, 2012; Hudson and others, 2014). These latter studies, while demonstrating the potential for plume monitoring in Arctic fjord environments, have had a focus on melt-season, river-fed plumes (which enter a fjord at its surface, rather than at its base), mostly located in West Greenland. Plume monitoring therefore requires validation in a range of environments and in different seasons. In particular, remote studies of specific tidewater glacier plumes are almost entirely absent. Yet plumes, being the only visible expression of tidewater glacier runoff, constitute a link between ice-sheet hydrology and oceans that can be investigated remotely (Chu and others, 2012).

Consequently, the aim of this work is to evaluate the utility of frequent-repeat Moderate Resolution Imaging Spectroradiometer (MODIS) imagery for detecting and monitoring variation in plumes, as indicated by the Total Suspended Solids concentration (*TSS*) of surface waters, in the accessible glacier lagoon Jökulsárlón, Iceland. In-situ spectral reflectance and *TSS* measurements were made before the onset of the main melt season in April 2012. Correlation of reflectance and

TSS at all wavelengths is used to identify the most appropriate band of the MODIS instruments on board NASA's Terra/Aqua satellites (http://modis.gsfc.nasa.gov/), for mapping *TSS*. Plume variability from mid-April to the end of May 2012 is then identified and discussed in terms of the hydrologic development of Jökulsárlón.

CHARACTERISTICS OF JÖKULSÁRLÓN

Iceland is a high-latitude environment, where glaciers play an important role in hydrology, feeding major rivers and supplying more than 30% of total runoff (Björnsson and Pálsson, 2008). A general glacier recession since the end of the 19th century has accelerated in the last decade, such that the main ice caps are likely to lose up to 35% of their present volume by the middle of the 21st century (Jóhannesson and others, 2006; Bergström and others, 2007). Meltwater-derived runoff is projected to peak around the same time, before returning to present-day values around the end of this century (Jóhannesson and others, 2007).

Jökulsárlón itself (Fig. 1) is a 23 km^2 (2012) tidal lagoon in southeast Iceland, formed in the 1930s as the Breiðamerkurjökull outlet glacier of the Vatnajökull ice cap retreated from an overdeepening (Björnsson and others, 2001). Breiðamerkurjökull calves ~0.3 km^3 of ice into Jökulsárlón per year, and as the glacier retreats, the lagoon continues to grow, at a rate of up to 0.5 $km^2\ a^{-1}$. Further growth of Jökulsárlón is probable, as the glacier bed is below sea level for ~20 km upstream of its current terminus (Björnsson and others, 2001). Runoff from Breiðamerkurjökull directly enters Jökulsárlón, such that the deposition of glacial sediment within the lagoon has reduced deposition offshore, accelerating coastal erosion, which proceeded at a rate of 8.5 $m\ a^{-1}$ for much of the 20th century in the vicinity of Iceland's main road (Víkingsson, 1991; Jóhannesson, 1994).

DATA SOURCES AND METHODS

The *TSS* of surface waters in Jökulsárlón is here related to remotely-sensed surface reflectance via a simple, single-band, in-situ calibration. The lagoon was accessed by Zodiac boat over 20–22 April 2012; simultaneous surface-water samples and reflectance measurements (Fig. 1) were obtained on each of these 3 d. In total 15 mL × 500 mL surface-water samples were acquired, filtered through 0.45 μm cellulose-nitrate membranes and the total mass of suspended material determined gravimetrically. Surface reflectance was measured with an *Analytical Spectral Devices (ASD) Inc. HandHeld 2* spectroradiometer, using a 25° foreoptic. Prior to each measurement, reflectance spectra from a calibrated Spectralon tablet were collected, so that raw Digital Number measurements could be post-processed to absolute reflectances. At each location 5–12 (on average 8) near-nadir spectral measurements were made between 12:05 and 14:29 local time, and averaged to reduce the effects of variable sky and surface conditions.

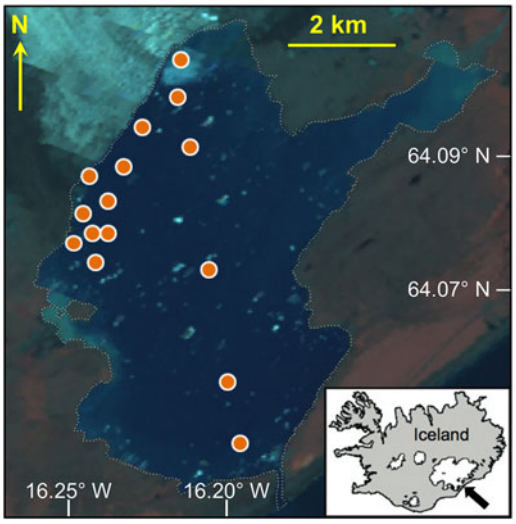

Fig. 1. Subset of a gap-filled, SLC-off Landsat 7 ETM+ scene, 28 May 2012, showing the locations of combined spectral measurements and water samples in Jökulsárlón. Inset shows location within Iceland.

Cloud-free imagery was initially identified from the NASA Rapid Response MODIS mosaic of the Arctic (http://lance-modis.eosdis.nasa.gov/imagery/subsets/?mosaic=Arctic), following which MOD09GQ (Terra) and MYD09GQ (Aqua) daily 250 m-resolution images were downloaded from the Reverb|ECHO service of NASA's Earth Observing System Data and Information System (EOSDIS; http://reverb.echo.nasa.gov/reverb). This level-2 imagery has been corrected for gases, aerosols and thin cirrus clouds (Vermote and Vermeulen, 1999). The images used were acquired between 11:56 and 13:55 local time (Table 1), giving near-nadir views with suitable solar illumination. The absence of cloud over Jökulsárlón itself was confirmed using the internal cloud algorithm flag of the 'state_1 km_1' QA layer in the imagery, which was processed in its native sinusoidal projection.

In order to obtain an up-to-date lagoon outline, a clear-sky Landsat 7 SLC-off scene (30 m-resolution) from 28 May 2012 was reprojected to the MODIS sinusoidal system (Fig. 1). The scene was gap-filled using the *Focal Analysis* tool within *Erdas Imagine* on a layer stack composed of all the band files except the thermal and panchromatic (http://landsat.usgs.gov/ ERDAS_Approach.php). Jökulsárlón was digitized from the resulting scene to obtain an Area of Interest (AOI) file, which could be used to subset MODIS images. To account for the lower spatial resolution of MODIS compared with Landsat, the AOI file was overlaid on a MODIS image and edited to remove mixed land/water pixels, leaving only water pixels. This also removes the potential for spurious high reflectances from coarser MODIS pixels at the lagoon edge containing both land and water. The final AOI file was used to subset appropriate MODIS images to the Jökulsárlón water surface.

In order to evaluate the effects of environmental conditions on plume characteristics, the following, further datasets were acquired. Time series of tidal heights for Hornafjörður (64°9.000′N, 15°7.200′W), 48 km northeast of Jökulsárlón on Iceland's southern coast, were obtained from the www Tide and Current Predictor (http://tbone.biol.sc.edu/tide/, using Xtide 2 software, http://www.flaterco.com/). Tidal tendency ($\Delta tide$, positive for flood and negative for ebb tides) was then calculated for the time of image acquisition. Coastal weather data (hourly air temperature, T_a, and precipitation, P) for the Kvísker weather station (WMO number 4886, 63° 57.576′N, 16° 5.465′W, 30 m a.s.l.) 13 km southwest of Jökulsárlón, were supplied by Veðurstofa Íslands. Because of the highly localized nature of wind regimes, wind velocity (V_w) and direction data were obtained from a University of Iceland Automatic Weather Station located

Table 1. Plume and associated environmental descriptive statistics for all days on which usable MODIS images are available: acquisition time (UTC), air temperature (T_a), rainfall in 24 h up to acquistion time (P_{24}), Positive Degree Hours (ΣPDH, cumulative from 1 April 2012), tidal tendency ($\Delta tide$), wind direction (D_w), meridional wind velocity (V_w; positive is offshore, negative is onshore), proportional lagoon coverage by floating ice (*%ice*), proportional lagoon coverage by turbid plume (*%plume*), minimum Total Suspended Solids (*TSS*) value in plume (TSS_{min}), mean TSS value in plume (TSS_{mean}), standard deviation of TSS values in plume (TSS_σ)

	19 Apr	26 Apr	27 Apr	02 May	07 May	10 May	11 May	15 May	16 May	28 May	30 May
Acq^n time	12:32	12:38	13:21	13:55	12:20	12:51	11:56	13:09	12:14	12:38	12:26
T_a (°C)	5.4	3.2	8.1	9.7	3.6	7.6	11.2	3.0	4.3	13.9	8.2
P_{24} (mm)	1.0	0.0	0.0	0.0	0.0	0.0	0.0	0.0	0.0	0.2	0.0
ΣPDH	1407	1977	2039	3006	3509	3721	3879	4465	4512	6649	7069
$\Delta tide$ (m h^{-1})	−0.045	0.000	−0.201	−0.131	0.147	0.164	−0.155	−0.104	−0.080	−0.191	−0.158
D_w (°)	*No data*	215	28	11	13	24	172	351	6	22	22
V_w (m s^{-1})	*No data*	−0.54	0.96	2.05	7.35	3.69	−0.74	10.04	9.15	2.50	1.95
%ice	8.2	10.1	5.4	3.5	5.2	3.3	6.1	1.6	3.5	1.4	0.9
%plume	22.6	35.1	57.4	33.4	71.3	20.5	40.5	97.9	93.9	43.8	40.2
TSS_{min} (g L^{-1})	0.000	0.000	0.027	0.000	0.030	0.022	0.019	0.156	0.107	0.099	0.084
TSS_{mean} (g L^{-1})	0.124	0.139	0.224	0.143	0.273	0.128	0.172	0.223	0.249	0.189	0.185
TSS_σ (g L^{-1})	0.129	0.150	0.133	0.144	0.138	0.104	0.118	0.061	0.085	0.099	0.093

on Breiðamerkurjökull itself (64°11.757′N, 16°22.123′W, 570 m a.s.l.)

RESULTS AND ANALYSIS

The *TSS* of surface-water samples ranged from 0.17 to 0.58 g L^{-1} (Table 1). The corresponding reflectance varies with wavelength, although there is a consistent response (reflectance increasing with *TSS*) in a window that corresponds to MODIS band 1 (B1, 620–670 nm; Fig. 2a). *TSS* and reflectance are well correlated ($r = 0.86$) in this wavelength window: here the correlation plateau is very broad and clear (Fig. 2b), suggesting little benefit from further examination of derivative spectra. The strong correlation between in-situ-sampled *TSS* and 620–670 nm reflectance gives confidence that the B1 reflectance can be calibrated to values of *TSS*, using the relationship

$$TSS = 4.7004ref$$

($R^2 = 0.74$, $p = 0.00$) where *ref* is reflectance in B1 or the 620–670 nm wavelength window (Fig. 2c; Chen and others, 2015). This simple calibration has the benefit of being linear for the range of *TSS* sampled in April 2012, with no indication of the reflectance saturation observed in some comparable studies, for example, Chu and others (2009), who also measured higher reflectances for a given *TSS* (presumably a function of lithology and/or particle-size distribution).

The days of in-situ sampling were consistently overcast, so in-situ reflectances cannot be compared with MODIS reflectances directly. But using the calibration, it is possible to map *TSS* variability in the lagoon for cloud-free days. Allowance needs to be made for the presence of floating ice, mainly in the form of icebergs calved from the terminus of Breiðamerkurjökull, which will raise the average reflectance values of the pixels they occupy. It was therefore assumed that the highest *TSS* sampled (0.58 g L^{-1}) was a maximum for the lagoon, and that the corresponding reflectance value (0.13) was a maximum for non-ice-occupied water. The visual survey of the lagoon that was undertaken during in-situ measurements suggests that this is a reasonable assumption. B1 greyscale images were then subsetted to the Jökulsárlón water surface using the Landsat-derived AOI, and pixels with a reflectance >0.13 were masked in order to remove high values likely to reflect iceberg presence. The location most consistently masked was close to the tidal inlet/outlet, where icebergs become grounded in shallow water.

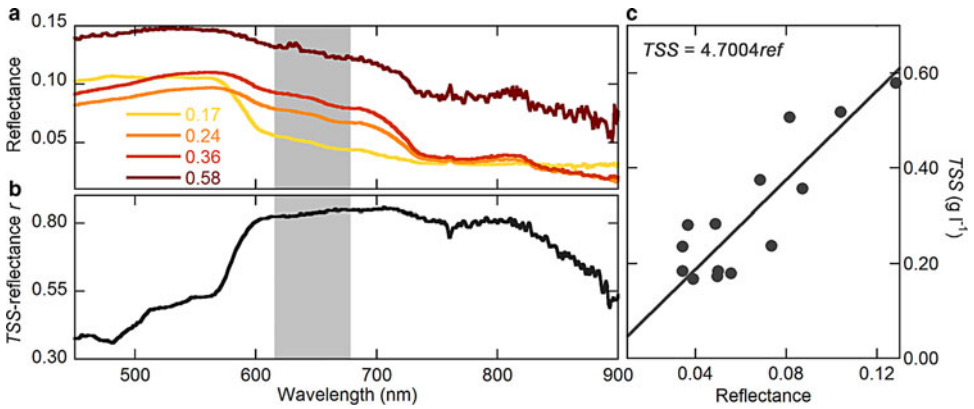

Fig. 2. (a) Wavelength vs. reflectance for different values of Total Suspended Solids (*TSS*, g L^{-1}), showing the consistent response in MODIS band 1 (B1), which is indicated by grey shading. (b) Wavelength vs. *TSS*-reflectance correlation, showing the consistent, high values in B1. (c) Regression of *TSS* on in-situ reflectance (*ref*) in a 620–670 nm window, equivalent to B1. The regression equation, $TSS = 4.7004ref$, is used to calibrate MOD09GQ imagery to *TSS* values, as described in the text.

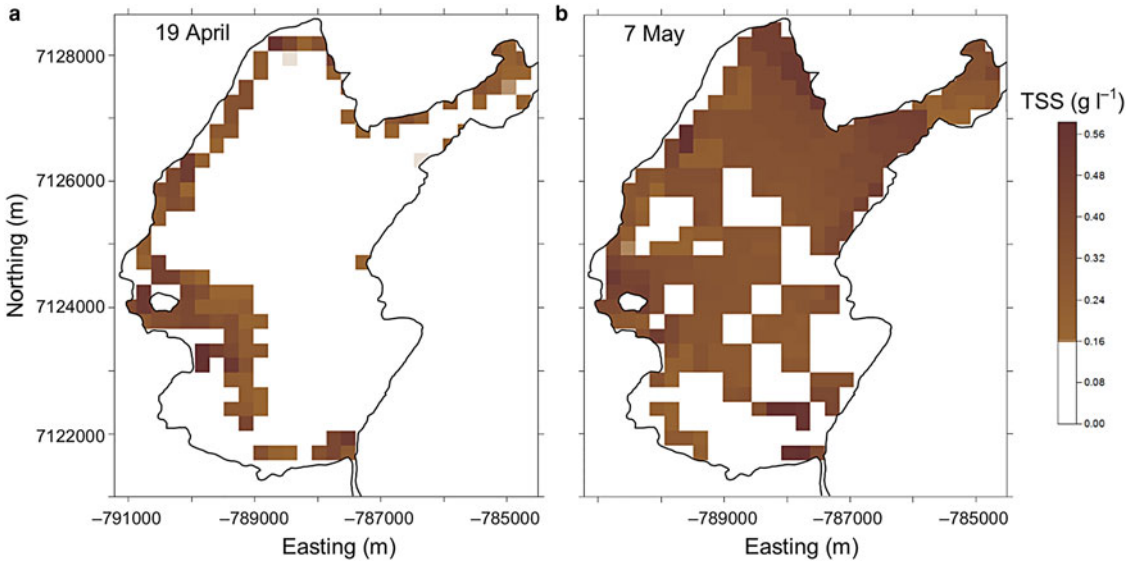

Fig. 3. (a) Plume extent and *TSS* distribution, 19 April 2012, the day of lowest TSS_{mean}. (b) Plume extent and *TSS* distribution, 7 May 2012, the day of highest TSS_{mean}.

The B1 calibration and high-value mask were used to map *TSS* variability in Jökulsárlón for all cloud-free days up to the end of May 2012. A potential change in the form of the *TSS*-reflectance relationship is anticipated as runoff to the lagoon increases significantly in the main melt season, June–September. The time series is not therefore extended into that period, since there is evidence for significant seasonality in the hydrographic properties and processes of Jökulsárlón. Brandon and others (2013) and Voytenko and others (2015a) found comparable lagoon water temperatures (0.5–2.5°C) in spring and summer 2012, respectively. However, summer salinities (7–17 psu) were lower than in spring (15–21 psu), indicating a clear dilution effect from summer melting and runoff. Moreover, Brandon and others (2013) observed Gade slopes in springtime temperature-salinity plots (Gade, 1979), denoting submarine melting at the terminus of Breiðamerkurjökull, whereas in summer Voytenko and others (2015a) did not, concluding as a result that there was a seasonal shift in melting from mainly ocean forcing in winter and spring, to mainly atmosphere forcing in summer and autumn.

Eleven clear-sky days yielded usable imagery, covering the period 19 April–30 May. MOD09GQ images were used for all days except 2 May, when the MOD09GQ image was cloud-affected so an MYD09GQ image was used instead. All images used were acquired within a daily 2 h window ~1300 coordinated universal time (UTC; Table 1). Figure 3 shows *TSS* maps for the days, which exhibited the lowest (19 April) and highest (7 May) mean values of plume *TSS*. Also shown for the same days is the proportion of the lagoon that is covered by an identifiable plume, which is defined with a threshold value of $TSS = 0.16$ g L^{-1}, equivalent to a B1 reflectance of 0.03 (Fig. 2): this corresponds to the minimum *TSS* sampled, which was the lowest concentration that could be detected visually in-situ. Isolated 'plume' pixels were masked, as they were probably subject to ice contamination elevating reflectance values, unless they intersected the lagoon boundary, where they were likely to represent point sources of turbid water input.

Figure 3 shows turbid runoff inputs to the northern shore of Jökulsárlón from Breiðamerkurjökull, at both the east and particularly the west margins. There are also turbid, terrestrial river inputs to the lagoon, again from the east and especially the west margins. This corresponds to the pattern observed in-situ. Riverine inputs have a glacial origin and are not distinguishable from submarine inputs in this analysis. There are further high *TSS* values adjacent to the tidal inlet, where strong turbulence is encountered in shallow water (<20 m). This fundamental spatial pattern is essentially unchanging over the period studied, although the relative contributions of these various sources change significantly, with turbid inputs from the east margin of Breiðamerkurjökull, for example, being notably high on 7 May (Fig. 3).

DISCUSSION

Time series of plume variables, tides and meteorology are presented in Figure 4. Plume metrics such as area and length have previously been measured as proxies for hydrologic outputs from the land to the ocean (Thomas and Weatherbee, 2006; Halverson and Pawlowicz, 2008; Lihan and others, 2008) but not often for glacially-fed plumes (Chu and others, 2009; McGrath and others, 2010; Hudson and others, 2014). The proportion of Jökulsárlón that is covered by an identifiable plume ($\%_{plume}$) varies between 23 and 98% over the interval considered (Table 1), but with no significant temporal trend ($\%_{plume} = 0.0057–0.24d$, $R^2 = 0.08$, $p = 0.41$, where d is Day of Year). Likewise, although mean *TSS* (mean of all unmasked pixels, TSS_{mean}) is greater at the end of the observation interval than at the start, there is no significant trend in that variable either ($TSS_{mean} = 0.017 + 0.0013d$, $R^2 = 0.11$, $p = 0.33$). However, minimum plume *TSS* (TSS_{min}, which is not co-linear with TSS_{mean}) does increase significantly in the same interval ($TSS_{min} = 0.0030d - 0.34$, $R^2 = 0.52$, $p = 0.01$). Correlations between the plume variables, tides and meteorology are presented in Table 2. In general, there are few simple associations between the series. For instance, there are no significant correlations between air temperature, 24 h precipitation or tidal tendency and any *TSS* metrics. Further, there is no association between the plume-covered proportion of the lagoon and tidal tendency.

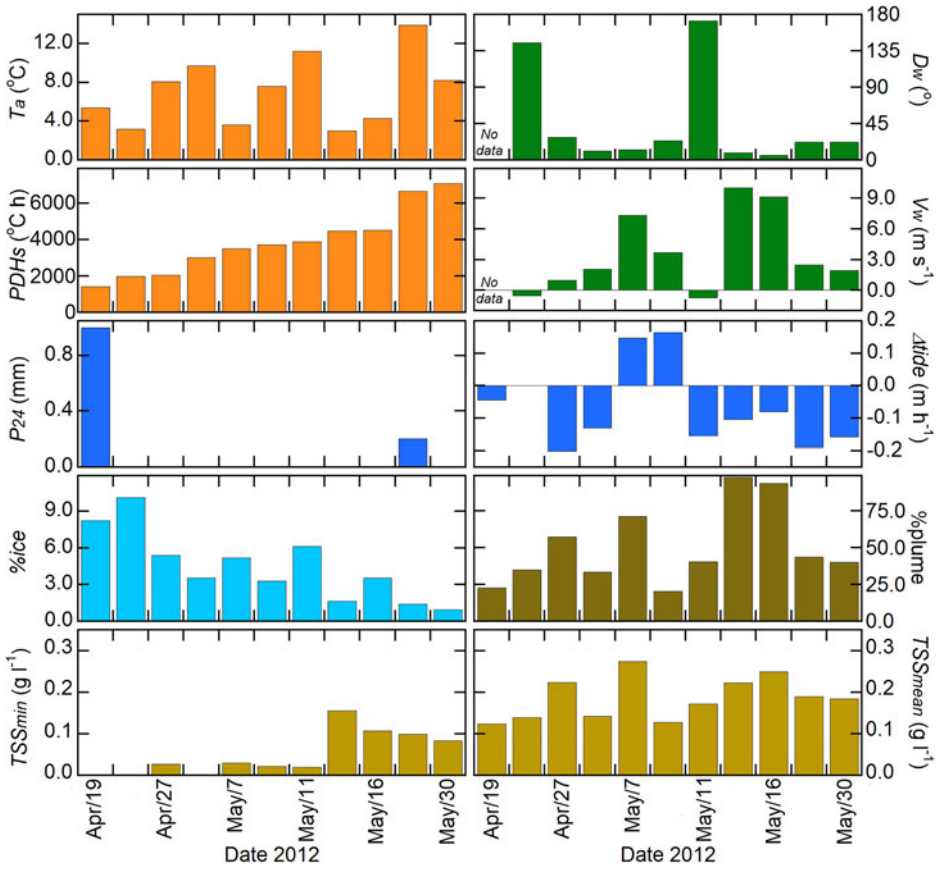

Fig. 4. Values of environmental variables and plume metrics for the 11 d on which imagery was available. The date axis simply shows available days sequentially: it does not show actual time intervals. Refer to Table 1 caption for explanation of the variables. Temperature-related variables are shown in orange, wind-related variables in green, lagoon variables in blues and plume metrics in browns. Note that D_w is expressed as the difference from North, hence small values are offshore, large values are onshore. Also note that *%ice* and *%plume* have different vertical scales, but TSS_{min} and TSS_{mean} share a vertical scale.

The only variables with which TSS_{mean} is significantly correlated are $\%_{plume}$ and V_w (positive correlations in both cases; Table 2). The standard deviation of plume *TSS* (TSS_σ), on the other hand, is not significantly correlated with $\%_{plume}$, but is significantly, positively correlated with the ice-covered proportion of the lagoon ($\%_{ice}$, simply quantified as those pixels with reflectance >0.13). TSS_σ is also significantly, negatively correlated with both Σ*PDH* and wind speed (Table 2). TSS_σ also exhibits a strong, negative correlation with TSS_{min}, but this is a constraint of the threshold mask used to define maximum plume *TSS*. Maximum plume *TSS* is not therefore a very useful metric, but the TSS_{min} threshold is only used to define the plume extent, not to constrain *TSS* values, and is more useful as a result. In fact, TSS_{min} exhibits correlations that suggest the plume metrics do capture the pre-melt-season evolution of the lagoon: Σ*PDH* is significantly, positively correlated with TSS_{min}, while $\%_{ice}$ is significantly, negatively correlated with it (Table 2). This suggests that MODIS-derived metrics are credibly representing rising overall turbidity in the lagoon as melting accumulates.

The lack of correlation between Σ*PDH* and TSS_{mean} may be influenced by the application of the maximum *TSS* threshold, but this is not likely to be the only influence. *TSS* is controlled by sediment availability, which is limited (Hodgkins and others, 2003). Therefore, maximum *TSS* will increase seasonally only to a certain level before stabilising or even declining as sediment supplies diminish. As this occurs, changes in total sediment fluxes are likely to be expressed through changes in plume extent, rather than in plume *TSS* values. Indeed, Chu and others (2009) observed seasonal hysteresis between ice-sheet melt extent and plume area,

Table 2. Pearson product-moment correlation coefficient, *r*, for plume and associated environmental descriptive statistics

	TSS_{mean}	TSS_σ	TSS_{range}	TSS_{min}	*%ice*	*%plume*	T_a	P_{24}	Σ*PDH*	Δ*tide*	D_w	V_w
TSS_{range}	*−0.47*	***0.87***	*1.00*									
TSS_{min}	*0.54*	***−0.91***	***−0.95***	*1.00*								
%ice	−0.33	**0.72**	0.55	**−0.72**	*1.00*							
%plume	**0.86**	−0.55	**−0.75**	**0.74**	−0.33	*1.00*						
Σ*PDH*	0.28	−0.66	−0.52	**0.69**	**−0.83**	0.21	0.42	−0.34	*1.00*			
V_w	**0.65**	**−0.62**	**−0.65**	**0.68**	−0.38	**0.84**	**−0.59**	−0.13	0.17	0.32	0.20	*1.00*

Significant values ($p < 0.05$) are in bold, potentially co-linear values are in italics. Rows in which no significant correlations occur have been omitted.

suggesting late-season, sediment-supply exhaustion. This emphasises the value of our linear reflectance-*TSS* calibration, which can be used to map values of TSS and suggests that the approach taken here, of basing the maximum reflectance threshold on high, ice-proximal *TSS* values observed in April, is reasonable, as it is unlikely that sediment supply and therefore maximum *TSS* will markedly increase as the melt season progresses.

The temporal trend in $\%_{ice}$ is significant ($\%_{ice} = 77.103–0.0019d$, $R^2 = 0.69$, $p = 0.00$) and it is negatively associated with ΣPDH ($r = -0.83$; Table 2), but this is probably explained by the circulation of icebergs around and out of the lagoon, rather than by melt processes: in particular, a cluster of icebergs in the southwest of Jökulsárlón moves anti-clockwise to the outlet and largely disperses over the course of the observed interval, accounting for most of the ice-cover decrease. Voytenko and others (2015b) noted that the large-scale circulation within Jökulsárlón was mostly clockwise, but that there was also the occasional formation of small-scale, anti-clockwise eddies near the shore, of which the movement of this iceberg cluster is probably an example.

The cloudiness associated with an extended period of rainfall gives an 11 d gap in the MODIS series from 16 May. *TSS* values are lower (TSS_{mean} 0.19 g L^{-1}) than those pre-gap (TSS_{mean} 0.25 g L^{-1}) when the data resume (Table 1, Fig. 4). Melt rates tend to be low during rainfall, as cloudiness reduces receipts of solar radiation; this is despite rising air temperatures at Kvísker, where the persistent cloud cover contributes to a reduced diurnal temperature range. A plausible interpretation of the reduced post-gap *TSS* is that the extended period of recession flow during the days of cloud and rainfall reduces sediment entrainment, and therefore also the volume and turbidity of runoff to the lagoon in late May, though values are still higher than at the beginning of the observation interval in late April. Actual runoff from Breiðamerkurjökull, being mostly submarine, is unknown. While T_a and ΣPDH are reasonable proxies for melt rates and cumulative melt respectively, neither are satisfactory proxies for runoff itself due to the complexity of the glacier drainage system, with its time-varying storage properties (e.g. Hodgkins and others, 2013).

As plumes disperse down a fjord or estuary, their characteristics are often increasingly influenced by tides (Bowers and others, 1998; Halverson and Pawlowicz, 2008) and winds (Stumpf and others, 1993; Whitney and Garvine, 2005). Dowdeswell and Cromack (1991) found that plume extent in Signehamna, Svalbard, was tidally dominated; wind speed and direction had little influence in the small (<1 km^2), sheltered inlet they studied. However, in the much larger Kangerlussuaq Fjord, West Greenland, Chu and others (2009) noted that the tidal influence on plume extent was negligible, as shown by nearly-identical plume-extent probability-distribution functions during incoming and outgoing tides. Any effect of tides on plume formation in Jökulsárlón is potentially affected by a constricting effect on water leaving the lagoon, but not on entering it (Tinder, 2012). This produces a more rapid rise in water level during the rising tide and a slower decrease during the falling tide.

V_w here is significantly correlated with all the plume metrics, but to the greatest degree (and positively) with $\%_{plume}$. The 3 d of strongest winds coincide with the 3 d of greatest plume extent (Fig. 4). The wind direction on all of these days is offshore (351–13°). There are 2 d when the MODIS image is acquired during onshore winds (172°–215°) but these do not correspond with notably low $\%_{plume}$ – which might be expected, given that strong offshore winds correspond with high $\%_{plume}$. However, onshore winds are somewhat weaker than offshore ones, with mean onshore velocities at the time of image acquisition being 0.71 m s^{-1} (corresponding to a meridional wind stress of 0.001 kg m^{-1} s^{-2}), compared with offshore velocities of 4.87 m s^{-1} (meridional wind stress 0.038 kg m^{-1} s^{-2}).

The influence of tidal tendency on the extent of the plume is therefore quantifiably less than that of the wind regime: $\Delta tide$ is negative on two of the three largest plume days, but strongly positive on the other, while V_w is consistently high on all three. This also suggests that the constricting effect of falling tides probably does not have an important influence on plume extent. Whitney and Garvine (2005) indicated that moderate-to-strong winds could modify the width of a large, coastal river plume significantly, and even overwhelm the general, buoyancy-driven flow. With reference to simple calculations by Voytenko and others (2015b), katabatic wind speeds measured on Breiðamerkurjökull are sufficient to sustain a wind-driven circulation within the surface waters of Jökulsárlón: wind speeds about half the magnitude of the offshore ones can account for most of the observed surface current speeds.

CONCLUSIONS

This study demonstrates that MODIS band 1 reflectance (620–670 nm) can successfully be related to *TSS* values for a tidewater glacier meltwater outflow plume. Similar relationships have previously been identified (e.g. Chu and others, 2009; Hudson and others, 2014), but this study differs in applying to a specific overturning plume at a calving face, as opposed to plumes derived from subaerial, glacially-fed river runoff, or to fjord systems as a whole. Furthermore, the simple, single-band calibration at Jökulsárlón is linear, without the signal saturation identified in some other studies from glacial environments. This requires application of an in-situ-sampling-constrained threshold to determine plume extent, but aids water quality mapping, in that a wider range of plume metrics can be determined, for example, pixel-by-pixel *TSS* and statistical measures of its variability, instead of simply an index of its presence or absence. The 250 m-resolution of the MODIS imagery does not impose any apparent limitations in this 23 km^2 lagoon system: the remotely-identified spatial variability in the turbid plume corresponds to that observed in-situ. Significant trends in several plume metrics are readily identified in the pre-melt-season interval for which the calibration can confidently be applied. Plume extent responds principally to forcing by surface winds, as tidal influence appears limited in the lagoon, and the offshore wind regime of the Breiðamerkurjökull area is consistently strong.

Further work should determine the plume's inter- and intra-annual variability, and water-source discrimination (e.g. subglacial *vs*. subaerial inputs). Plumes hold potential, if not necessarily as proxies for runoff, then as indices of hydrological outputs, in large-scale, ungauged or ungaugeable systems. Results from Jökulsárlón suggest that remote studies of plumes also have potential for quantifying sediment fluxes, though further work is required to determine the degree of any (presumably location-specific) relationship

between plume extent and depth: previous, oceanographic studies of plumes in glacial fjords (e.g. Cottier and others, 2005; Sciascia and others, 2013) suggest that stratification is sufficiently consistent that this is probably feasible.

ACKNOWLEDGEMENTS

G. Gísladóttir, Veðurstofa Íslands, supplied the Kvísker weather data. F. Pálsson, Institute of Earth Sciences, University of Iceland, supplied the Breiðamerkurjökull weather data. Financial support was provided by the School of Social, Political and Geographical Sciences, Loughborough University, by the Open University, and by the Percy Sladen Memorial Fund, Linnean Society of London. J. Chandler, Department of Civil and Building Engineering, Loughborough University, provided access to *Erdas Imagine*. J.A. Runólfsson, Jökulsárlón ehf, was an extremely helpful Zodiac pilot. The constructive comments of Allen Pope and an anonymous reviewer led to significant improvements to the original manuscript.

REFERENCES

Arendt KE and 6 others (2011) Effects of suspended sediments on copepods feeding in a glacial influenced sub-Arctic fjord. *J. Plankton Res.*, **33**, 1526–1537 (doi: 10.1093/plankt/fbr054)

Bergström S and 31 others (2007) Impacts of climate change on river runoff, glaciers and hydropower in the Nordic area. *Joint Final Report from the CE Hydrological Models and Snow and Ice Groups. CE Rep. No.* 6, The CE Project, Reykjavík

Björnsson H and Pálsson F (2008) Icelandic glaciers. *Jökull*, **58**, 365–386

Björnsson H, Pálsson F and Gudmundsson S (2001) Jökulsárlón at Breiðamerkursandur, Vatnajökull, Iceland: 20th century changes and future outlook. *Jökull*, **50**, 1–18

Bowers DG, Boudjelas S and Harker GEL (1998) The distribution of fine suspended sediments in the surface waters of the Irish Sea and its relation to tidal stirring. *Int. J. Remote Sens.*, **14**, 2789–2805

Brandon M, Hodgkins R, Björnsson H and Ólaffson J (2013) Hydrographic measurements in Jökulsárlón lagoon, Iceland. *Am. Geophys. Union* [Abstr. OS11A-164]

Chen S and 5 others (2015) Estimating wide range Total Suspended Solids concentrations from MODIS 250-m imageries: an improved method. *ISPRS J. Photogramm. Remote Sens.*, **99**, 58–69 (doi: 10.1016/j.isprsjprs.2014.10.006)

Chu VW (2013) Greenland ice sheet hydrology: a review. *Prog. Phys. Geog.*, **38**(1), 1–36 (doi: 10.1177/0309133313507075)

Chu VW and 5 others (2009) Sediment plume response to surface melting and supraglacial lake drainages on the Greenland ice sheet. *J. Glaciol.*, **55**, 1072–1082 (doi: 10.3189/002214309790794904)

Chu VW, Smith LC, Rennermalm AK, Forster RR and Box JE (2012) Hydrologic controls on coastal suspended sediment plumes around the Greenland ice sheet. *Cryosphere*, **6**, 1–19 (doi: 10.5194/tc-6-1-2012)

Church JA and 13 others (2013) Sea level change. In Stocker TF and 10 others eds. *Climate change 2013: the physical science basis. Contribution of working group I to the fifth assessment report of the intergovernmental panel on climate change*. Cambridge University Press, Cambridge, UK and New York, NY, USA

Cottier F and 5 others (2005) Water mass modification in an Arctic fjord through cross-shelf exchange: the seasonal hydrography of Kongsfjorden, Svalbard. *J. Geophys. Res.*, **110**(C122005) (doi: 10.1029/2004JC002757)

Curran PJ and Novo EMM (1988) The relationship between suspended sediment concentration and remotely sensed spectral radiance: a review. *J. Coastal Res.*, **4**(3), 351–368

Dowdeswell JA and Cromack M (1991) Behavior of a glacier-derived suspended sediment plume in a small Arctic inlet. *J. Geol.*, **99**, 111–123

Doxaran D, Froidefond J-M, Lavender S and Castaing P (2002) Spectral signature of highly turbid waters: application with SPOT data to quantify suspended particulate matter concentrations. *Remote Sens. Environ.*, **81**(1), 149–161 (doi: 10.1016/S0034-4257(01)00341-8)

Gade HG (1979) Melting of ice in sea water: a primitive model with application to the Antarctic ice shelf and icebergs. *J. Phys. Oceanogr.*, **9**(1), 189–198 (doi: 10.1175/1520-0485(1979)009<0189:MOIISW>2.0.CO;2)

Halverson MJ and Pawlowicz R (2008) Estuarine forcing of a river plume by river flow and tides. *J. Geophys. Res.*, **113**(C09033) (doi: 10.1029/2008JC004844)

Hodgkins R, Cooper R, Wadham J and Tranter M (2003) Suspended sediment fluxes in a high-Arctic glacierised catchment: implications for fluvial sediment storage. *Sed. Geol.*, **162**, 105–117

Hodgkins R, Cooper R, Tranter M and Wadham J (2013) Drainage-system development in consecutive melt seasons at a polythermal, Arctic glacier, evaluated by flow-recession analysis and linear-reservoir simulation. *Water Resour. Res.*, **49**(7), 4230–4243 (doi: 10.1002/wrcr.20257)

Hu C and 5 others (2004) Assessment of estuarine water-quality indicators using MODIS medium-resolution bands: initial results from Tampa Bay, FL. *Remote Sens. Environ.*, **93**(3), 423–441 (doi: 10.1016/j.rse.2004.08.007)

Hudson B and 5 others (2014) MODIS observed increase in duration and spatial extent of sediment plumes in Greenland fjords. *Cryosphere*, **8**(4), 1161–1176 (doi: 10.5194/tc-8-1161-2014)

Jóhannesson H (1994) Coastal erosion near the bridges across Jökulsá á Breiðamerkursandi in southeastern Iceland. In Viggósson G ed. *Proceedings of the international coastal symposium*, Höfn, The Icelandic Harbour Authority, Iceland, 405–414

Jóhannesson T and 14 others (2006) The impact of climate change on glaciers and glacial runoff in the Nordic countries. In *Proc. European Conference of Impacts of Climate Change on Renewable Energy Sources*, Reykjavík, Iceland

Jóhannesson T and 13 others (2007) Effect of climate change on hydrology and hydro-resources in Iceland. *Final Report of the VO-Project*, OS–2007/011

Joughin I, Alley R and Holland D (2012) Ice-sheet response to oceanic forcing. *Science*, **338**, 1172–1176 (doi: 10.1126/science.1226481)

Lihan T, Saitoh S-I, Iida T, Hirawake T and Iida K (2008) Satellite-measured temporal and spatial variability of the Tokachi River plume. *Estuarine Coastal Shelf Sci.*, **78**(2), 237–249 (doi: 10.1016/j.ecss.2007.12.001)

McGrath D and 5 others (2010) Sediment plumes as a proxy for local ice-sheet runoff in Kangerlussuaq Fjord, West Greenland. *J. Glaciol.*, **56**(199), 813–821 (doi: 1 0.3189/002214310794457227)

Miller RL and McKee BA (2004) Using MODIS Terra 250 m imagery to map concentrations of total suspended matter in coastal waters. *Remote Sens. Environ.*, **93**(1–2), 259–266 (doi: 10.1016/j.rse.2004.07.012)

Sciascia R, Straneo F, Cenedese C and Heimbach P (2013) Seasonal variability of submarine melt rate and circulation in an East Greenland fjord. *J. Geophys. Res.*, **118**(5), 2492–2506 (doi: 10.1002/jgrc.20142)

Statham PJ, Skidmore M and Tranter M (2008) Inputs of glacially derived dissolved and colloidal iron to the coastal ocean and implications for primary productivity. *Global Biogeochem. Cy.*, **22**, 1–11 (doi: 10.1029/2007GB003106)

Straneo F and 15 others (2013) Challenges to understand the dynamic response of Greenland's marine terminating glaciers to oceanic and atmospheric forcing. *Bull. Am. Met. Soc.*, **94** (doi: 10.1175/BAMS-D-12-00100.1)

Stumpf RP, Gelfenbaum G and Pennock JR (1993) Wind and tidal forcing of a buoyant plume, Mobile Bay, Alabama. *Cont. Shelf Res.*, **13**(11), 1281–1301

Tedstone AJ and Arnold NS (2012) Automated remote sensing of sediment plumes for identification of runoff from the Greenland ice sheet. *J. Glaciol.*, **58**(210), 699–712 (doi: 10.3189/2012JoG11J204)

Thomas AC and Weatherbee RA (2006) Satellite-measured temporal variability of the Columbia River plume. *Remote Sens. Environ.*, **100**(2), 167–178 (doi: 10.1016/j.rse.2005.10.018)

Tinder P (2012) *Ocean-ice interactions at Breiðamerkurjökull glacier, Southeast Iceland*. (Unpublished MSc thesis, Ohio State University, USA)

Vermote EF and Vermeulen A (1999) Atmospheric Correction Algorithm: Spectral Reflectances (MOD09). Version 4.0. *Algorithm Technical Background Document*, NASA Contract NAS5-96062, 107 pp

Víkingsson S (1991) The south coast of Iceland. Shoreline changes according to maps and photographs. *Orkustofnun*, OS-91042/VOD-07 B, 7 pp (in Icelandic)

Voytenko D and 7 others (2015a) Multi-year observations of Breiðamerkurjökull, a marine-terminating glacier in southeastern Iceland, using terrestrial radar interferometry. *J. Glac.*, **61**(225), 42–54 (doi: 10.3189/2015JoG14J099)

Voytenko D and 5 others (2015b) Observations of inertial currents in a lagoon in southeastern Iceland using terrestrial radar interferometry and automated iceberg tracking. *Comp. Geosci.*, **82**, 23–30 (doi: 10.1016 /j.cageo.2015.05.012)

Whitney MM and Garvine RW (2005) Wind influence on a coastal buoyant outflow. *J. Geophys. Res.*, **110**(C03014) (doi: 10.1029/2003JC002261)